Proceedings of the
Annual Stability Conference
Structural Stability Research Council
Toronto, Canada, March 25-28, 2014

Experimental and computational analysis of direct torsion in cold-formed steel lipped channels

K. D. Peterman[1], G. Bian[2], B. W. Schafer[3]

Abstract

The objective of this paper is to provide benchmark results and explanatory shell finite element models for the direct torsion behavior of a cold-formed steel lipped channel. Although the theory for elastic torsional response of a thin-walled cold-formed steel lipped channel member is well-developed, little exists in terms of experimental benchmarks that test this theory and even less on situations beyond the elastic theory, including torsional buckling, torsional yielding, and full plastification in torsion. Since warping is the primary deformation mode resisting torsion, member end conditions are of particular importance. Here, a typical cold-formed steel lipped channel member is loaded experimentally in direct torsion. The torsion is applied directly to a plate welded to the ends of the lipped channel. End plates of 1 in. [25.4 mm] were observed to provide warping fixed end conditions, while 1/4 in. [6.4 mm] plates provide a semi-rigid end condition. In addition to end fixity, the effect of standard punched holes and member length were also explored experimentally. Shell finite element models were completed in ABAQUS to shed additional light on the experimental results and further explore the effect of end fixity on torsional behavior. In addition, classical expressions for torsional stiffness, buckling, and yielding are compared with the experiments and models. The long-term goal of the research is to incorporate torsional response directly into cold-formed steel member design.

1. Introduction

In typical structural member beam design, transverse loads are applied so that the resultant force passes through the centroid of the cross section. If the cross section is doubly symmetric, torsion will not occur because the centroid and the shear center coincide. In general; however, cold-formed steel beams consist of open sections where

[1] Graduate Research Assistant, Department of Civil Engineering, Johns Hopkins University, Baltimore, MD <kpeterm1@jhu.edu>
[2] Graduate Research Assistant, Department of Civil Engineering, Johns Hopkins University, Baltimore, MD <bian@jhu.edu>
[3] Professor and Chair, Department of Civil Engineering, Johns Hopkins University, Baltimore, MD <schafer@jhu.edu>

the centroid and shear center do not coincide. When transverse load is applied away from the shear center, it causes torque. In the general case of an unsymmetric open thin-walled cross-section, this torque is resisted by both shear and longitudinal (warping) stresses and is termed to be in a state of non-uniform torsion.

It is common for thin-walled members to develop torsion capacity exceeding the yield torque, T_y, even nearing the plastic torque, T_p. Although elastic torsional response of cold-formed steel lipped channel members are well-studied, the extent to which inelastic reserve exists in commonly used cold-formed steel sections subjected to torsion, or combined bending and torsion has not been studied extensively.

AISI–S100-12 provides design criteria for a singly or doubly symmetric member that is subjected to torsional loading. For torsionally unrestrained flexural members subjected to both bending and torsional loading, the available flexural strength is multiplied by a reduction factor R as shown in Eq. 1.

$$R = \frac{f_{bending\text{-}max}}{f_{bending} + f_{torsion}} \leq 1 \quad (1)$$

Where $f_{bending\text{-}max}$ is the bending stress at extreme fiber; $f_{bending}$ is the bending stress at the location in cross section where combined bending and torsion stress is at its maximum; and $f_{torsion}$ is the torsional warping stress at the location in cross section where combined bending and torsion stress is at its maximum. Additional details area available in AISI-S100-12, but in general this provides a reduction similar to a longitudinal stress-based linear interaction equation. The AISC Steel Design Guide (AISC, 2003) *"Torsional Analysis of Structural Steel Members"* describes the effect of torsion and how the resulting elastic stresses can be calculated. Inelastic reserve capacity under torsion is not considered in AISI or AISC design specifications.

To elucidate the basic behavior of cold-formed steel under direct torsion, we performed a series of benchmark tests for the direct torsion behavior of cold-formed steel lipped channels. In addition, we performed complementary shell finite element models of the tests. The shell finite element models are presented, and torsional yielding, full plastification, and torsional buckling for the member are all explored. The results are important for future cold-formed steel design of the torsional, as well as combined bending and torsional, response of cold-formed steel members.

2. Experimental configuration

Using an MTS tension-torsion load cell outfitted with hydraulic grips, cold-formed steel channel sections were welded to end plates and installed in the rig as shown in Figure 1. The specimens were loaded in pure torsion, with the bottom grip loading the specimen while the top remained fixed. No sensors other than the load cell force and rotation were employed.

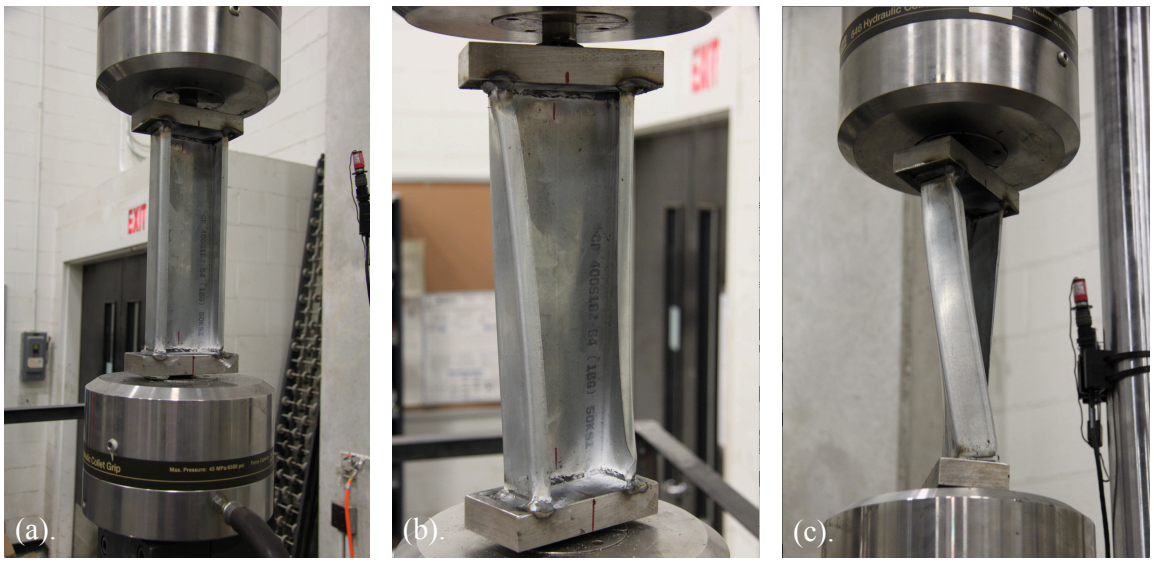

Figure 1: (a) unloaded specimen in rig (b) moderately loaded specimen (c) specimen loaded with maximum 45 degree angle of rotation.

2.1 Test specimen

The CFS specimens were cut from a single punched 400S162-54 (50 ksi [345 MPa] stud 22 feet [6.7 m] in length. This cross section was chosen based upon material availability and steel thickness, as 54 mil steel is commonly used for shear wall and gravity wall construction. Lengths of channel section were then welded to steel plates to form rigid (1 in. [25mm] end plate) and semi-rigid (0.25 in [6.4mm] end plate) end conditions. To connect to the testing rig, steel shafts were welded to the end plates, as shown in Figure 2.

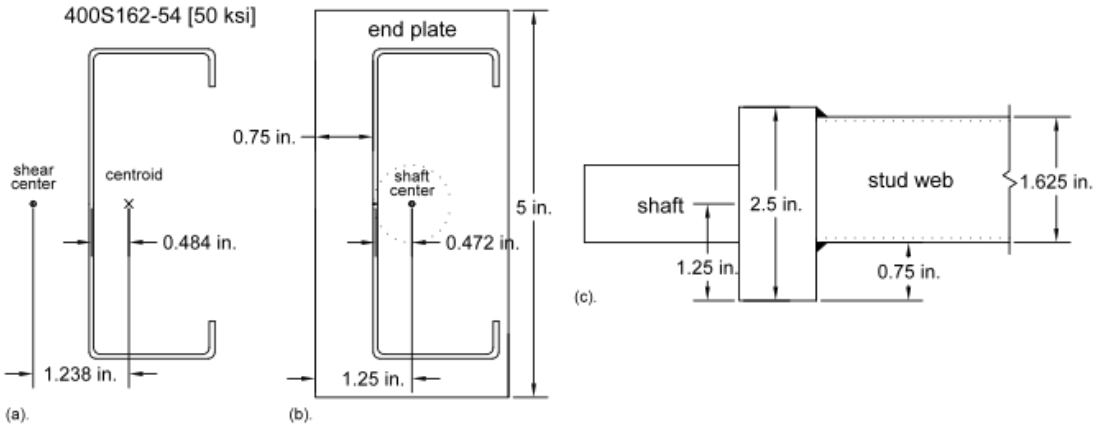

Figure 2: Test specimen

The shafts were aligned with the cross-section to coincide with the centroid of the section. As Figures 2(a) and 2(b) demonstrate, the shaft center and centroid do not perfectly coincide, but are within 2.5% of ideal.

2.2 Test matrix

Three parameters were varied experimentally: end plate thickness (resulting in "rigid" and "semi-rigid" boundary conditions), specimen length, and effect of holes. Tests 4, 5, and 6, identical save for the load rate in test 5, establish a core set of results for the section with rigid end conditions.

Table 1: Material properties

Specimen	Hole	Length (in.)	End plate	Notes
1	-	12	0.25	shakedown
2	-	12	2 x 0.25	shakedown
3	-	12	0.25	N/A
4	-	12	1.00	N/A
5	-	12	1.00	15 min load rate
6	-	12	1.00	N/A
2H	✔	12	0.25	N/A
4H	✔	12	1.00	N/A
1H2	✔	24	0.25	N/A

1 in. = 25.4 mm

Specimens 1 and 2 were conducted for shake-down purposes only, no results from these tests are presented in this paper.

2.3 Load protocol

Specimens were monotonically loaded to a rotation of 45 degrees in 30 minutes (exceptions are noted in Table 1), corresponding to a load rate of 0.025 degrees per second or 0.00044 radians per second. Once a 45 degree rotation was achieved, the specimen was unloaded at a rate of 0.75 degrees per second.

3. Experimental results

Numerical results for the experimental testing are shown in Table 2 below. Photographs of failure modes for representative specimens are shown in Figure 3. As anticipated, the rigid specimens achieved higher torsional moment values than the semi-rigid specimens. For the identical rigid specimens (tests 4, 5, and 6), yield rotation was almost identical though corresponding torsional moments vary slightly. These rigidly connected specimens experienced inelastic lip local buckling past yield (Figure 3(b)) and ultimately, failed in the weld between channel and end plate (Figure 3(c)).

Table 2: Experimental results

Specimen	Hole	Length (in.)	End plate	K_o	K_f	θ_y	T_y	θ_u	T_u
				kip-inch/degree	*kip-inch/degree*	*degree*	*kip-inch*	*degree*	*kip-inch*
3	-	12	0.25	0.34	0.08	8.29	2.83	44.98	5.26
4	-	12	1.00	1.09	0.03	4.11	4.49	34.04	5.50
5	-	12	1.00	1.19	0.04	4.11	4.90	31.63	5.94
6	-	12	1.00	1.03	0.06	4.14	4.27	29.14	5.82
4H	✔	12	1.00	0.34	none	10.74	3.60	17.02	3.70
1H2	✔	24	0.25	0.11	0.05	14.20	1.51	45.00	2.99

1 kip = 4.45 kN, 1 in. = 25.4 mm

The semi-rigid specimens experienced end plate stability failures as a result of warping forces generated by the specimens in torsion (Figure 3(a)). Test 3 demonstrated similar lip local buckling as in tests 4-6, however the response is significantly more ductile.

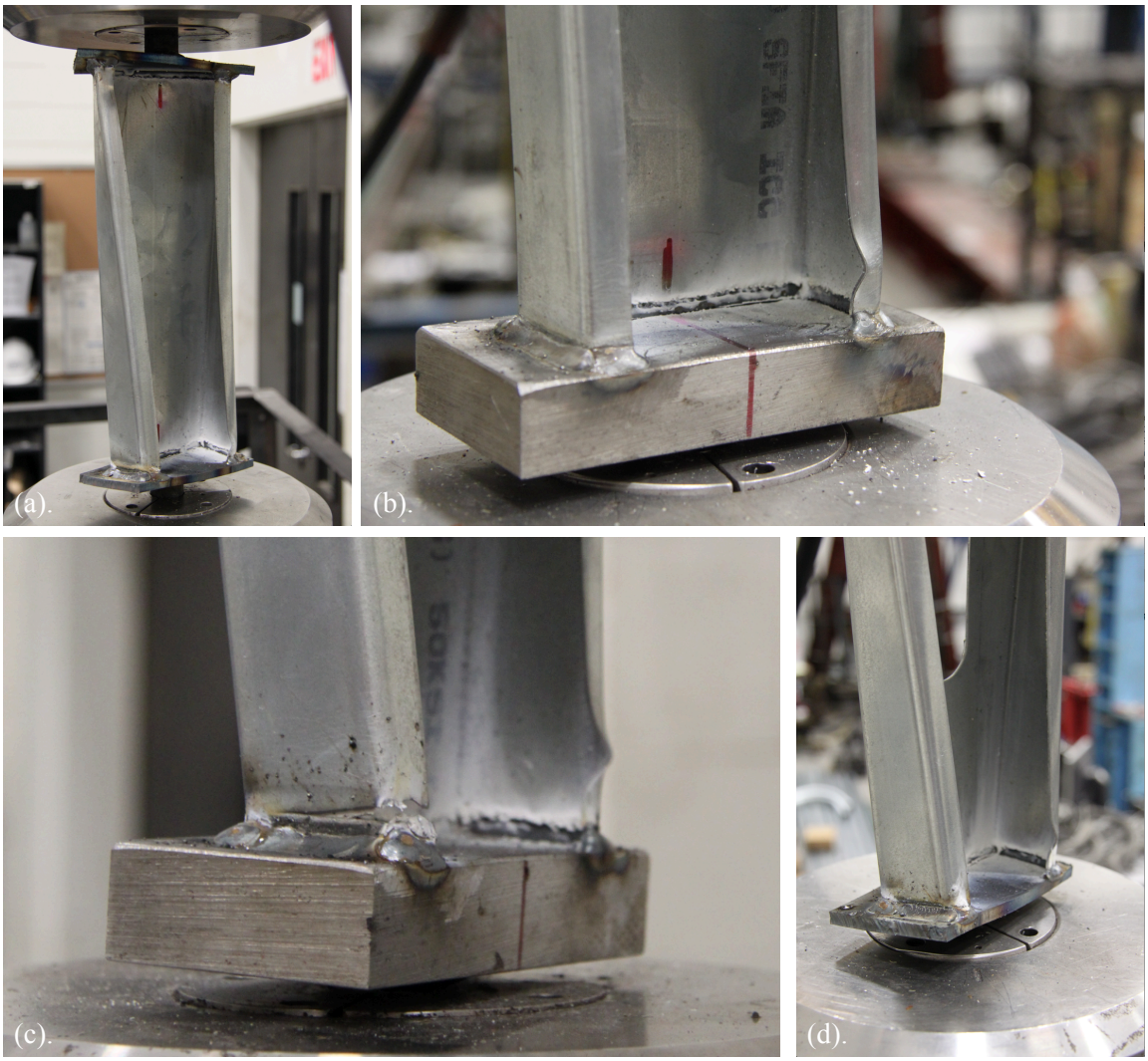

Figure 3: Failure modes of specimens (a) test 3, demonstrating the semi-rigid end plates buckling due to warping forces in the channel section induced by torsion (b) test 4, depicting inelastic lip local buckling past yield (c) test 6, depicting the rigid specimen failure post-peak with both lip local buckling and failure along the opposing weld (d) test 3, demonstrating the influence of holes for the semi-rigid end condition and showing lip local buckling post-yield.

The 24 in. [0.6 m] specimen, test 1H2, demonstrated only slight lip local buckling at the maximum 45 degree rotation. This specimen did not reach the yield torsional moment before the rotational limits of the machine were reached.

4. Finite element model configuration

To evaluate the test results and further explore the cold-formed steel channel properties, finite element analysis was carried out in ABAQUS. The analysis focused on three different models of the 400S162-54 [50ksi] stud in torsion: (i) the stud with 1 in. [25.4

mm] endplate plus loading shaft, (ii) the stud with 1/4 in. [6.4 mm] endplate plus loading shaft, and (iii) an isolated model of the stud with completely warping fixed end conditions.

4.1 Material characterization and element selection

The stress-strain relationship in the ABAQUS model was based on a direct tensile test, as shown in Fig. 4. Material nonlinearity was accounted for using classical metal plasticity theory based on von Mises yield criterion and isotropic hardening. Here we used the 0.2% offset method to obtain the material yield stress from the tensile test curve. The yield stress, Young's modulus, and other material properties are provided in Table 3.

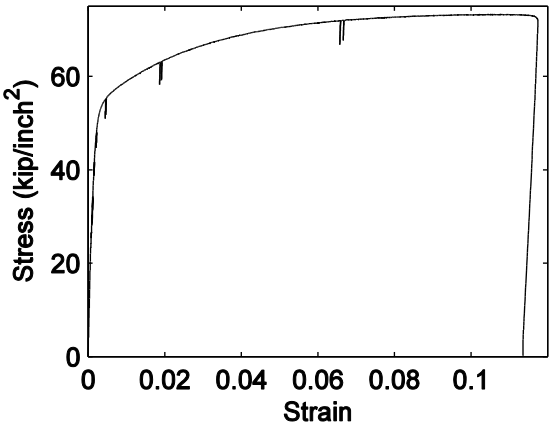

Figure 4: Stress-strain relation for the ABAQUS model (1 ksi = 6.895 MPa)

In ABAQUS, the engineering (nominal) stress/strain values ($\sigma_{nom}/\varepsilon_{nom}$) are converted to true stress/strain values ($\sigma_{true}/\varepsilon_{true}$) by the following equations:

$$\varepsilon_{true} = \ln(1 + \varepsilon_{nom}) \tag{2}$$

$$\sigma_{true} = \sigma_{nom}(1 + \varepsilon_{nom}) \tag{3}$$

Table 3: Material properties

Material	F_y	F_u	ε_u	E	ν
	ksi	ksi	-	ksi	-
from 400S162-54	54.1	80.1	0.09	29500	0.3

1 ksi = 6.895 MPa

Here, for purposes of simplification, modal imperfections and residual stresses were not considered in the finite element models, although they certainly exist from the manufacturing process and from the welding process to create the specimen.

The S4R shell element was used for modeling the stud and the C3D8R solid element was used for modeling the endplate and the loading shaft. Typical meshes are shown below.

4.2 End Conditions

The end conditions of the model had a significant effect on the computational result. Three different end conditions were considered in the finite element models: rigid ends, plated ends, and plated ends with a loading shaft.

In the rigid end model, Fig. 5, one end of the stud was coupled to a reference point with all six degrees of freedom fixed, while the other end of the stud was coupled to a reference point with five degrees of freedom fixed (all except for the twist degree of freedom). For the plated ends model, Fig. 6, there were two endplate thicknesses: 1 in. [25 mm] and 1/4 in. [6.4 mm]. The plates were explicitly included in the model. The loading shaft was added to the plated ends model resulting in the third model type as shown in Fig. 7.

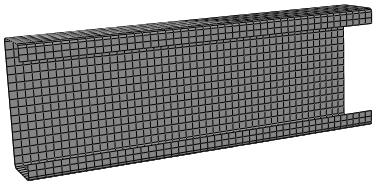

Figure 5: Model without endplate or shaft (stud only)

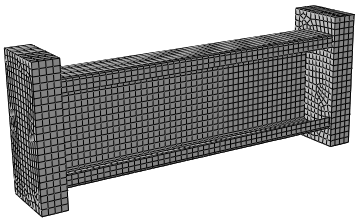

Figure 6: Model with endplate

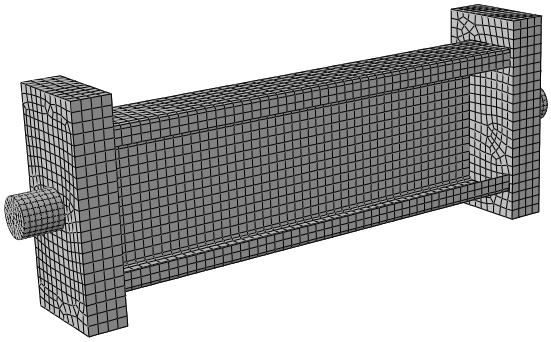

Figure 7: Model with endplate and loading shaft

In the test, the central axis of the shafts at both ends was lined up, under ideal conditions. However, imperfections in the location where the shaft was welded to the plate create the potential for perturbations from ideal at either end of the loading equipment, i.e., shaft offset can occur. To explore sensitivity to the loading axis offset, two different shaft offsets (Fig. 8) were modeled for both the 1 in. and ¼ in. plated ends model, from which reasonable maximum and minimum boundaries for the influence of shaft offset were obtained. The loading protocol considering shaft offset was completed in two steps in ABAQUS: first a translational displacement of the shaft end was given as the loading point offset; then the rotation was given based on the initial offset.

Four kinds of loading shafts, with different diameters as illustrated in Fig. 9, were also explored in the model to show the effect of shaft rigidity on the torsional results.

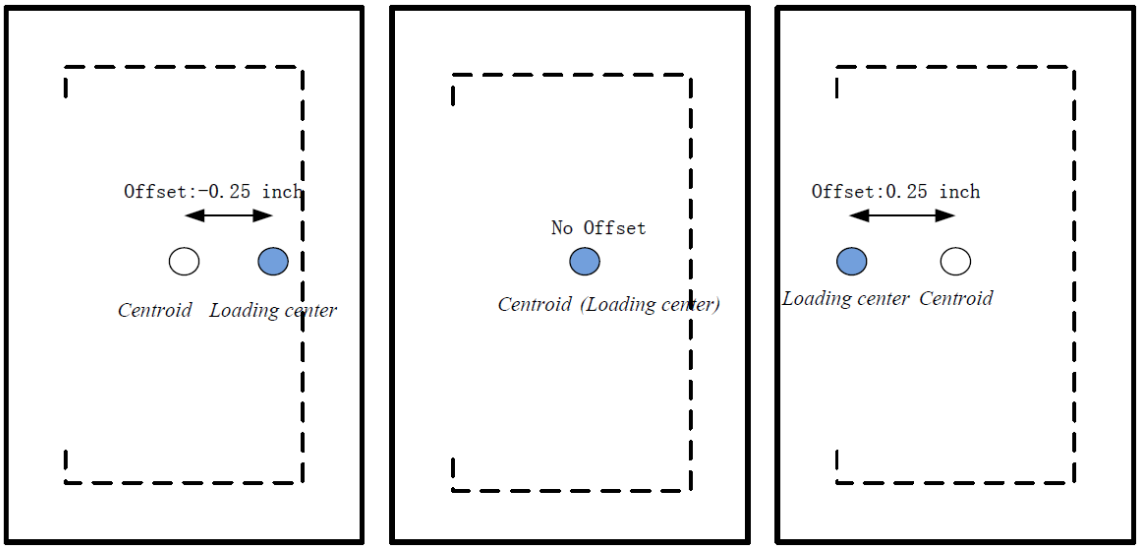

Figure 8: Loading shaft offset in model

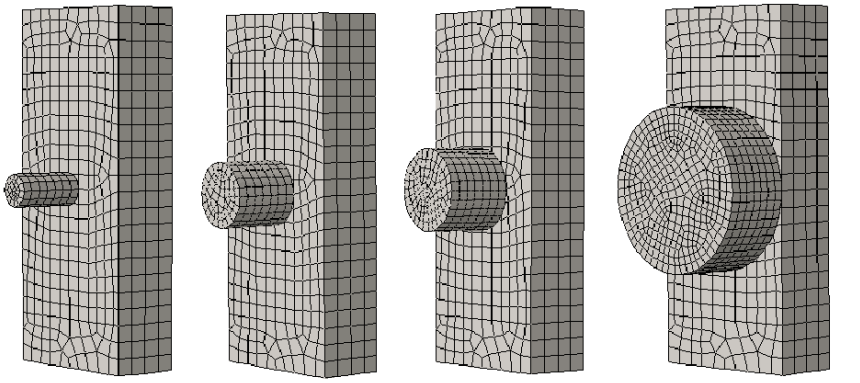

Figure 9: Different shaft diameters in model

5. Finite element results and analysis

Based on the model described in Section 4, we present in this section the basic results of the torsional FE analysis.

5.1 Influence of end conditions

As illustrated in Fig. 10, the torsional moment-angle relationship for models with different end conditions gives significantly different stiffness. The single stud model with the idealized warping fixed end, leads to the greatest stiffness (and much higher than test results). When the endplate was added to the model, the observed stiffness decreased due to the endplate deformation, but the stiffness was still greater than the test result. Finally, both the endplate and the loading shaft were considered in the model. This last model was most consistent with the test result. Therefore, we conclude that both the endplate and the loading shaft must be included in the model for comparison to the measured machine twist (localized experimental measurements of the member twist are not available).

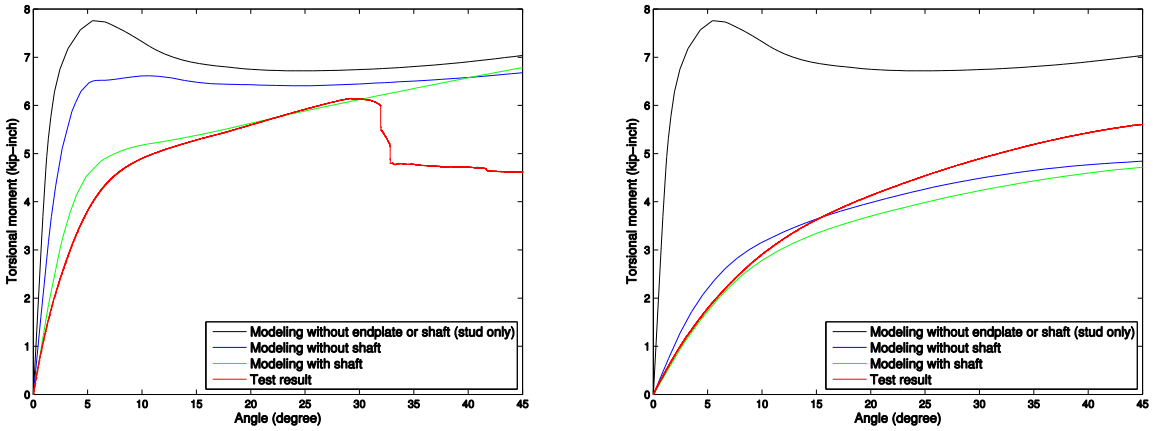

Figure 10: Torsional moment-angle relationship for one inch and one quarter inch endplates

The effect of shaft offset on the computational results is shown in Fig. 11. From the results we can conclude that shaft offset contributes to the potential experimentally observed scatter, but it is not a primary reason for differences between test and model.

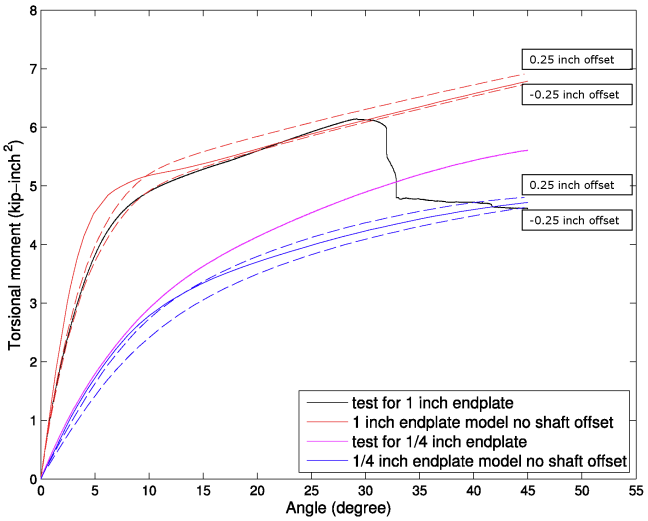

Figure 11: Loading shaft offset effect on the analytical result

Although the experiments were only conducted for a 1 in. diameter shaft, the shaft itself is a proxy for end fixity. As shown in Fig. 12, as the diameter increases, and when the diameter of the shaft is large enough, the results converge to the ideal model with perfect warping fixed end conditions. In contrast, when the diameter of the shaft is as small as 0.5 in. the stiffness decreases considerably.

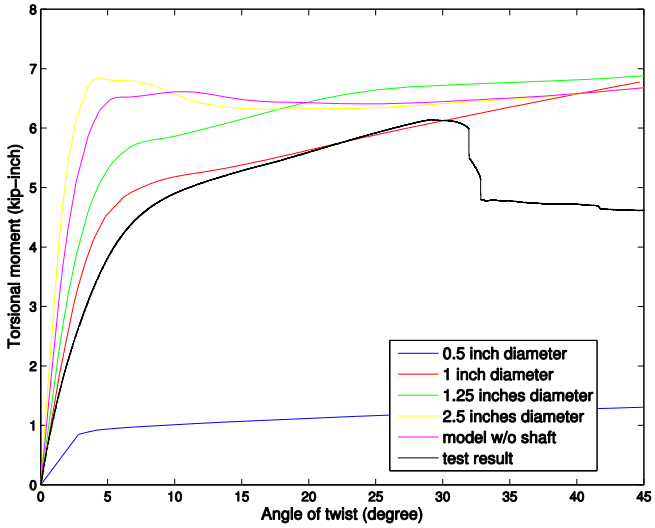

Figure 12: Shaft diameter effect on the model

5.2 Characterization of cross-section yielding and plasticity

The theory for elastic torsional response of thin-walled cold-formed steel lipped channel member was largely developed by Timoshenko (1961) and Vlasov (1961) etc. in the past century. Here we investigate this elastic response, and then extend the model into yielding to better understand the inelastic response in direct torsion.

In a member subjected to torsion, the torque at which the von Mises (effective) stress in the cross section first attains the flow (yield) stress is defined as the yield torque, T_y. (This is slightly different than considering only longitudinal warping stresses and setting them equal to F_y, as the shell FE model includes the full three-dimensional state of stress resulting from warping, shear, and even local plate bending and end effects). In the model (and test) first yield occurs at the end cross section because warping was restrained at both ends.

Therefore, we considered the torque–effective stress curve (or torque–effective strain curve) for the element that had the maximum stress (or strain) at the end cross-section along the member. The effective strain developed under torsion for the ideal stud model, 1 in. endplate and ¼ in. endplate models are shown in Fig. 13. The torque at which yielding initiates increases as the end becomes more rigid and for the ¼ in. end plate model is about 1 kip-in., for the 1 in. endplate model is 2 kip-in., and for the ideal warping fixed stud only model is 4 kip-in..

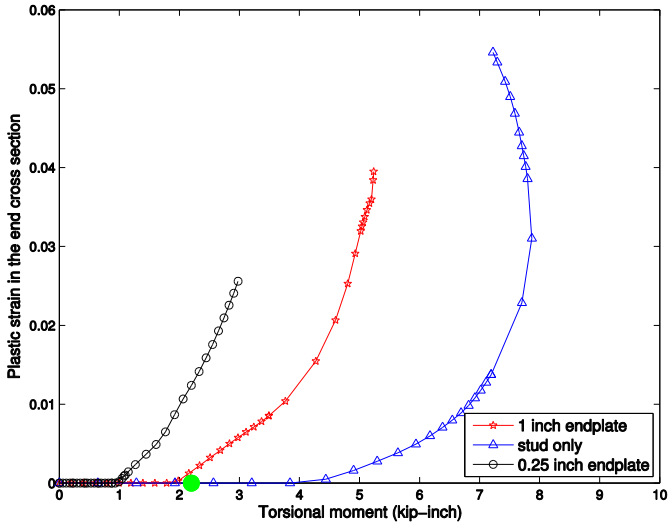

Figure 13: Plastic strain – torsional moment relationship

As the torque increases past T_y, more elements across the section yield. We define the torque at which all elements of the end cross section have reached their initial yield strain as the full plastic torque, T_p. The reserve capacity between T_y and T_p is potentially important for cold-formed steel design. Here we chose the elements at the end and middle cross sections of the member to study the plastic torque. We define a plasticity indicator function, I, for a single element in the cross section as:

$$I = \begin{cases} 1 & \varepsilon_p > 0 \\ 0 & \varepsilon_p = 0 \end{cases} \tag{4}$$

Where, ε_p is the effective plastic strain. $\varepsilon_p > 0$ implies the element has yielded and $\varepsilon_p = 0$ indicates the element is still elastic. For the element we use the maximum strain at the middle gauss point along the thickness of the cross section.

With the indicator function defined the plastic cross-section ratio, P, is:

$$P = \frac{\sum_{j=1}^{N} I_j}{N} \tag{5}$$

Where, I_j, is the plasticity indicator for element j in the cross section; and N is the number of elements around the cross section. The plastic cross section ratio, P, is 0 when the cross section is elastic and 1 when the cross section is full plastic. Fig. 14 provides the plastic cross section ratio, P, for the end and middle stud cross sections for both the 1 in. and ¼ in. endplate models vs. (a) rotation and (b) torsional moment. Plasticity initiates at the ends, and continues to be greatest at the ends throughout the twist. Plasticity develops more quickly in the member for the thicker (1 in.) endplate. Significant twist is required to plastify the section. Reserve between T_y and T_p is significant, but involves large twist.

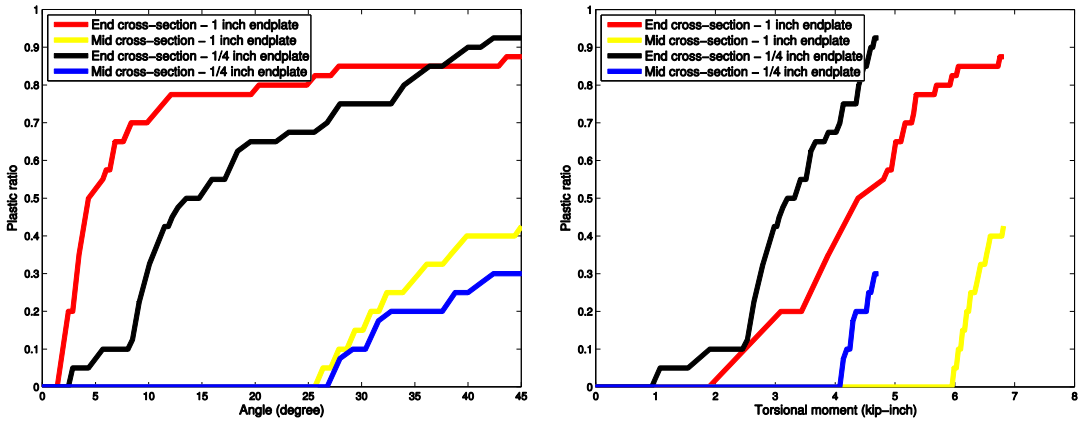

(a) (b)

Figure 14: Plastic cross section ratio vs. (a) rotation and (b) torsional moment.

5.3 Comparison with classical solutions

According to the cross section properties the bimoment, B, at which the cross section reaches first yield is 12.2 kip-in.^{2} (obtained from CUFSM (Schafer and Ádány 2006) model of the straight line cross section). From a simple beam element Mastan (McGuire et al. 2000) model of the test setup the yield torque can be obtained based on the bimoment: $T_y = 2.2$ kip-in. (Indicated as a green circle in Fig. 13). The classical solution, with warping fixed ends, reasonably approximates the more complex finite element analysis; although further studies are warranted.

5.4 *Torsional stability results*

A linear Eigen-buckling analysis was carried out for the 1 in. endplate, ¼ in. endplate, and single stud model to obtain the buckling mode, and critical torque $T_{cr.}$ The first five buckling modes are shown in Fig. 15. From the figure we can see that the first few buckling modes with the 1 in. and 1/4 in. endplates were similar, and localized at the ends. However, for the single stud model with idealized warping fixed end conditions, the buckling occurred in the member, only localizing in the 5th mode. T_{cr} for the different models are provided in Table 4, the critical torque is about 6-8 times T_y for each of the models. (A range where yielding, not buckling, would be expected to dominate).

Table 4: Critical torque for models with different end conditions

	T_{cr}		
Buckling Mode	stud only (kip)	1 in. endplate (kip)	¼ in. endplate (kip)
1st	18.7	15.8	8.4
2nd	18.9	15.8	8.5
3rd	22.6	18.6	11.0
4th	24.2	18.8	11.1
5th	29.5	19.5	13.0

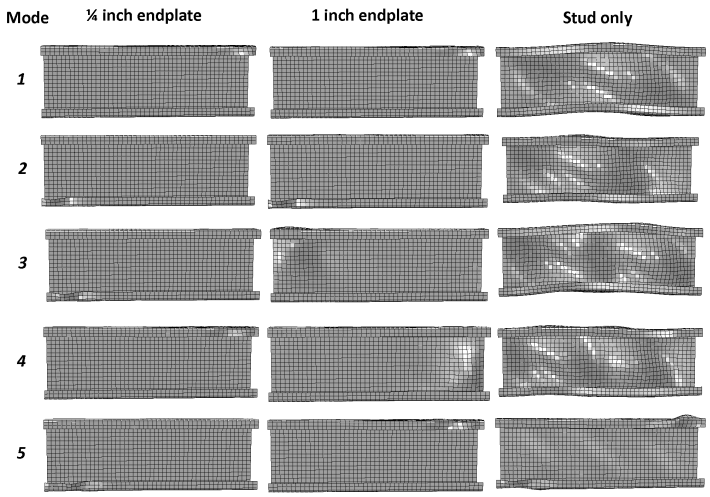

Figure 15: Buckling modes predicted by FE models

5.5 Inability to simulate members with holes in torsion

We also tried to evaluate the torsional behavior of the members with holes, as in the test. The analysis results showed that there was no apparent stiffness decrease in the torsional moment–angle curve, which deviated from the test result. Here, considering the different shear resistance character for the S4 and S4R element in ABAQUS, we tried both without difference. Accurate modeling of the influence of holes in torsion remains as future work.

6. Discussion and future work

Significant future work remains to develop an explicit torsional calculation for cold-formed steel member design. Specifically, the development of a Direct Strength Method style expression (Schafer 2008) for torsion is desired, where torsional nominal capacity is expressed as $T_n = f(T_{cr},T_y)$. However, given the importance of inelastic reserve it is expected that $T_n = f(T_{cr},T_y,T_p)$ will be required. Thus, further work developing T_p is needed. This work would be the first step towards examination of torsion in combined loading; specifically torsion and bending; and later expanding new ideas about beam-columns to also include torsion. Testing, further modeling, and analytical developments are all required.

7. Conclusions

This paper provides benchmark test results and explanatory shell finite element models for the direct torsion behavior of a cold-formed steel lipped channel. Tests of a standard cold-formed steel 400S162-54 [50ksi] stud were conducted in direct torsion by welding on endplates and a shaft and mounting in a tension-torsion universal testing machine. The tests indicate the importance of end boundary conditions on the torsional response. In addition, the tests demonstrate the impact of specimen length, and standard hole punchouts in the web, on torsional capacity. After significant twist, approximately 30°, inelastic local buckling initiates in the lip at the member end and the peak torsional capacity is reached.

Shell finite element models of the tests demonstrate that the torsional stiffness of the member in the test is large enough that the endplate and shaft must be explicitly included in the modeling even for 1 in. thick end plates and 1 in. diameter shafts. Sensitivity to shaft offset is also observed in the modeling, but not found to be significant for expected experimental error in assembly and testing. Exploration of yielding, plastificiation, and buckling in the shell finite element model lay the ground work for developing new design provisions that explicitly treat torsion. Classical solutions can provide the torque at yield and are verified with the shell finite element model. Plastification in torsion develops over large twists and the inelastic reserve between yielding and fully plastification is dramatic. Torsional buckling is sensitive to the end conditions, but generally several times greater than yielding – indicating the dominance of yielding, followed by inelastic buckling, in the final response. Work remains to develop explicit torsional provisions, but it is hoped that this research provides the first definitive steps in this direction.

Acknowledgments

The authors would like to thank the National Science Foundation (NSF-CMMI #1041578), American Iron and Steel Institute (AISI), ClarkDietrich, Steel Stud Manufacturers Association, and the Steel Framing Industry Alliance, The views expressed in this work are those of the authors and not NSF, AISI, or any of the participating companies or advisors. Testing was performed at the Structural Engineering and Earthquake Simulation Laboratory (SEESL) at the University at Buffalo. The authors would like to thank the SEESL staff for their expertise and cooperation.

References

AISI-S100-12 (2012). North American Specification for the Design of Cold-Formed Steel Structural Members. American Iron and Steel Institute. Washington, D.C.

ABAQUS. ABAQUS/Standard User's Manual, Version 6.9EF1. Pawtucket, RI; 2009.

Timoshenko, S. P., Gere, J. M. (1961). *Theory of Elastic Stability*. McGraw-Hill

Vlasov, V. Z. (1961). *Thin-walled elastic beams*. Jerusalem Publication.

Schafer, B.W., Ádány, S. (2006). "Buckling analysis of cold-formed steel members using CUFSM: conventional and constrained finite strip methods." *Proceedings of the Eighteenth International Specialty Conference on Cold-Formed Steel Structures*, Orlando, FL. 39-54.

McGuire, W., Gallagher, R., Ziemian, R. (2000). *Matrix Structural Analysis, with MASTAN2,* Wiley & Sons, Inc., <MASTAN2 maintained at www.mastan2.com>.

Schafer, B. W. (2008). 'Review: The direct strength method of cold-formed steel member design.' *Journal of Constructional Steel Research*, 64(7), 766-778.